
Simulation-based inference using surjective sequential neural likelihood estimation

Simon Dirmeier*

Swiss Data Science Center
ETH Zurich, Switzerland

Carlo Albert

Swiss Federal Institute of Aquatic
Science and Technology, Switzerland

Fernando Perez-Cruz

Swiss Data Science Center
ETH Zurich, Switzerland

Abstract

We present Surjective Sequential Neural Likelihood (SSNL) estimation, a novel method for simulation-based inference in models where the evaluation of the likelihood function is not tractable and only a simulator that can generate synthetic data is available. SSNL fits a dimensionality-reducing surjective normalizing flow model and uses it as a surrogate likelihood function which allows for conventional Bayesian inference using either Markov chain Monte Carlo methods or variational inference. By embedding the data in a low-dimensional space, SSNL solves several issues previous likelihood-based methods had when applied to high-dimensional data sets that, for instance, contain non-informative data dimensions or lie along a lower-dimensional manifold. We evaluate SSNL on a wide variety of experiments and show that it generally outperforms contemporary methods used in simulation-based inference, for instance, on a challenging real-world example from astrophysics which models the magnetic field strength of the sun using a solar dynamo model.

1 Introduction

Probabilistic models are essential tools in the sciences to draw conclusions from data and to make decisions based on computational inferences. In the natural sciences, especially in disciplines such as biology, physics or psychology, Bayesian inference has become particularly popular due to its ability both to quantify uncertainty in parameter values using probability statements and to incorporate prior knowledge about quantities of interest. Bayesian statistics infers statistical parameters θ by conditioning the elicited prior distributions $p(\theta)$ on data y yielding a posterior distribution $p(\theta | y) \propto p(y | \theta)p(\theta)$. If the likelihood function $p(y | \theta)$ is available, i.e., tractably computable, conventional Bayesian inference using Markov chain Monte Carlo or variational methods can be used for parameter inference [Brooks et al., 2011, Wainwright and Jordan, 2008]. However, for many scientific hypotheses, the likelihood is not easy to compute and the experimenter merely has access to a simulator function $sim(\theta)$ that can generate synthetic data conditionally on a parameter configuration θ . In this case, simulation-based inference (SBI, Cranmer et al. [2020]) is a frequently applied alternative to still be able to conduct statistical experiments. Traditionally, statistical modellers have resorted to approximate Bayesian computation (ABC, Sisson et al. [2018]), and most successfully sequential Monte Carlo (SMC-ABC; e.g., Beaumont et al. [2009], Del Moral et al. [2012]) and variants thereof to infer approximate posterior distributions [Pritchard et al., 1999, Ratmann et al., 2007, Albert et al., 2015, 2022].

*Correspondence to: simon.dirmeier@sdsc.ethz.ch

However, ABC methods are computationally intensive and scale poorly to higher-dimensional settings. Furthermore, they require to define an appropriate small number of summary statistics beforehand which requires significant domain knowledge and which in some scenarios do not even necessarily exist. Recently, methods that are based on neural density or density-ratio estimation have found increased application in the natural sciences due to their reduced computational cost and convincing off-the-shelf performance [Brehmer et al., 2018, Delaunoy et al., 2020, Hermans et al., Brehmer, 2021, Dax et al., 2021].

Among these, generally three different branches of methods exist. Likelihood-based methods [Papamakarios et al., 2019, Glöckler et al., 2022] fit a surrogate model for the likelihood function using neural density estimators [Germain et al., 2015, Papamakarios et al., 2017, 2021] which allows to do conventional Bayesian inference and which has been shown to bring significant performance gains in comparison to ABC methods with the same computational budget. Cranmer et al. [2015], Durkan et al. [2020], Hermans et al. [2020], Thomas et al. [2022] and Miller et al. [2022] developed similar methods that instead target the likelihood-to-evidence ratio rather than the likelihood while Papamakarios and Murray [2016], Lueckmann et al. [2017], Greenberg et al. [2019] and Deistler et al. [2022] developed methods that try to approximate the posterior distribution directly.

In the case of likelihood-based methods, the accuracy of posterior inferences might suffer due to the inability of neural density estimators to correctly approximate the surrogate likelihoods, e.g., if the data are embedded in a low dimensional manifold but lie in a higher-dimensional ambient space or when the data contain non-informative data dimensions [Fefferman et al., 2016, Greenberg et al., 2019, Cunningham et al., 2020, Dai and Seljak, 2021, Klein et al., 2021].

To overcome this limitation, we present a new method for simulation-based inference which we call *Surjective Sequential Neural Likelihood* (SSNL) estimation. SSNL uses a surjective dimensionality-reducing normalizing flow to model the surrogate likelihood of a generative model by that allowing improved density estimation and consequently improved posterior inference, especially in high-dimensional settings. We demonstrate the method on several experiments highlighting in which scenarios dimensionality-reducing density estimators outperform recent methods such as SNL [Papamakarios et al., 2019] or automatic posterior transformation (APT, Greenberg et al. [2019]). Likewise, we outline when our method should not have a performance gain in comparison to the recent literature.

The structure of the manuscript is as follows. Section 2 describes background relevant for the introduced method and experiments. Section 3 introduces Surjective Sequential Neural Likelihood estimation. Section 4 shows the results on the conducted experiments and demonstrates the competitiveness of the method. Finally, Section 5 summarizes the contributions and discusses future researches of research in SBI.

2 Background

Given a parameter configuration $\theta \sim p(\theta)$, a simulator function $sim(\theta)$ is a computer program or experimental procedure that simulates an observable $y \leftarrow sim(\theta)$. Apart from stochasticity produced by $p(\theta)$, the simulator might be making use of another source of endogenous randomness. The simulator defines, albeit implicitly, a conditional probability distribution $p(y \mid \theta)$ to which the modeller does not have access or which they cannot evaluate in reasonable time. The goal of simulation-based inference [Cranmer et al., 2020] is to infer the posterior probability distribution $p(\theta \mid y) \propto p(y \mid \theta)p(\theta)$ for, in most cases, a specific sample y_0 which is typically an observation of some real-world process, e.g., describing some biological or physical phenomenon. The following section introduces some relevant concepts in SBI.

2.1 Density estimation using normalizing flows

Sequential density estimators such as SNL [Papamakarios et al., 2019] and APT [Greenberg et al., 2019] use conditional normalizing flows to fit a surrogate model to either approximate the intractable likelihood or the posterior which can then be used for conventional Bayesian parameter inference. Normalizing flows model a probability distribution via a pushforward measure as

$$q_f(\mathbf{y} \mid \boldsymbol{\theta}) = p(\mathbf{z}_0) \prod_k^K \left| \det J_k \right|^{-1} \quad (1)$$

where $\det J_k = \det \frac{\partial f_k}{\partial \mathbf{z}_{k-1}}$ is the determinant of the Jacobian matrix of the forward transformation f_k which is typically parameterized by a neural network ϕ_k . The forward transformations $f = (f_1, \dots, f_K)$ are a sequence of K diffeomorphisms and $p(\mathbf{z}_0)$ is some base distribution that has a density that can be evaluated exactly, for instance, a spherical multivariate Gaussian. The two densities q and p are related by the multiplicative term $\det J_k$ which is needed to account for the change-of-volume induced by f_k and which is termed likelihood contribution in Nielsen et al. [2020] and Klein et al. [2021]. The diffeomorphisms f_k are required to be dimensionality-preserving such that each of them has a respective inverse function to be able to both evaluate the probability of a datum and to draw samples which in practice can limit their expressivity and capacity to model high-dimensional data.

Each transformation f_k is composed of a *transformer* which can be any invertible function, and a *conditioner* which in the case of, e.g., masked autoregressive flows (MAFs, Papamakarios et al. [2017]) is typically a masked autoregressive network (MADE, Germain et al. [2015]) that ensures that the conditional density of the outputs of the network factorizes autoregressively. Note that we can choose each f_k to be a different operation, but here we choose them to be the same function, for instance, a shift-scale operation or, when a higher complexity is desired, a spline function [Durkan et al., 2019].

A conventional approach to introduce the conditioning parameter $\boldsymbol{\theta}$ to the forward transformation, i.e., to compute $f_k(\mathbf{z}_{k-1} \mid \boldsymbol{\theta})$, is by forwarding it through some additional embedding network, such as a single linear layer, and then adding it to either the input data \mathbf{z}_{k-1} or, respectively, to the output of the first hidden layer of ϕ_k . Sampling from a trained conditional normalizing flow $q_f(\mathbf{y} \mid \boldsymbol{\theta})$ requires to first sample (unconditionally or conditionally) from the base distribution $\mathbf{z}_0 \sim p(\mathbf{z}_0)$ and the pushing the sample forward through the conditional flow layers, such that $\mathbf{y} \leftarrow f_K \circ f_{K-1} \circ \dots \circ f_1(\mathbf{z}_0)$.

2.2 Sequential neural likelihood estimation

Sequential neural likelihood estimation [Papamakarios et al., 2019] iteratively fits a surrogate model using a conditional neural density estimator to approximate $q_f(\mathbf{y} \mid \boldsymbol{\theta}) \approx p(\mathbf{y} \mid \boldsymbol{\theta})$. SNL proceeds in R rounds: in the first round, $r = 1$, a sample of size N is simulated by iteratively evaluating $\text{sim}(\boldsymbol{\theta}_n)$ using prior draws $\boldsymbol{\theta}_n \sim p(\boldsymbol{\theta})$ yielding the data set $\mathcal{D} = \{\mathbf{y}_n, \boldsymbol{\theta}_n\}_{1 \dots N}^r$. The simulated data is used to train a conditional MAF as surrogate likelihood by maximizing the expected probability $\mathbb{E}_{\mathcal{D}}[q_f(\mathbf{y} \mid \boldsymbol{\theta})]$. Having access to a surrogate of the likelihood function, posterior realizations are generated either by sampling from $\hat{p}^r(\boldsymbol{\theta} \mid \mathbf{y}_0) \propto q_f(\mathbf{y}_0 \mid \boldsymbol{\theta})p(\boldsymbol{\theta})$ via Markov chain Monte Carlo [Brooks et al., 2011] or via optimization by fitting a variational approximation to the approximate posterior [Wiqvist et al., 2021]. SNL then uses the surrogate posterior as proposal prior distribution for the next round, $r + 1$, i.e., it draws a new sample of parameters $\boldsymbol{\theta}_n \sim \hat{p}^r(\boldsymbol{\theta} \mid \mathbf{y}_0)$ which are then used to simulate a new batch of pairs $\{\mathbf{y}_n, \boldsymbol{\theta}_n\}_{1 \dots N}^{r+1}$. The data sets from the previous rounds and the current round are then appended together and a new model is trained on the entire data set. With enough rounds R , samples per round N , and a sufficiently flexible density estimator q_f , SNL converges to the desired posterior distribution $p(\boldsymbol{\theta} \mid \mathbf{y}_0)$. Since one is in general interested in conditioning on a specific observation \mathbf{y}_0 , SNL builds the proposal prior for each round by composing a posterior that uses the observation of interest in the likelihood term.

SNL is flexible, unsurprisingly easy to implement, and has been shown to be competitive in comparison to methods that target the posterior in contrast to the likelihood or ABC methods [Papamakarios and Murray, 2016, Lueckmann et al., 2017, Beaumont et al., 2009], but suffers from performance degradation, e.g., if the data contain non-informative dimensions, as shown in Greenberg et al. [2019], and possibly if the data to be modelled lie on a lower-dimensional manifold inside a high-dimensional ambient space [Cunningham et al., 2020, Dai and Seljak, 2021, Klein et al., 2021].

2.3 Sequential neural posterior estimation

Sequential neural posterior estimation (SNPE) methods, e.g., automatic posterior transformation (APT, Greenberg et al. [2019]), instead use a normalizing flow to directly fit a surrogate model targeting the

posterior distribution thereby approximating $q_f(\theta | \mathbf{y}) \approx p(\theta | \mathbf{y})$ and by that effectively changing the roles of input and conditioning variables of the neural density estimator used in SNL. In similar fashion to SNL, APT models the approximate posterior distribution in a sequence of R rounds. In the first round, $r = 1$, a pair of samples of size N is drawn from the simulator and prior yielding a data set $\mathcal{D} = \{\mathbf{y}_n, \theta_n\}_{1 \dots N}^r$, and the flow is trained to maximize $\mathbb{E}_{\mathcal{D}}[q_f(\theta | \mathbf{y})]$. Subsequent rounds proceed by first composing a proposal prior as $\hat{p}^r(\theta) = q_f(\theta | \mathbf{y}_0)$, simulating new pairs $\{\mathbf{y}_n, \theta_n\}_{1 \dots N}^r$ where $\theta_n \sim \hat{p}^r(\theta)$ and then re-training the normalizing flow. Since the parameters are sampled from the proposal prior $\hat{p}^r(\theta)$ the surrogate posterior would no longer target the true posterior $p(\theta | \mathbf{y})$ but rather $q_f(\theta | \mathbf{y}) \propto p(\theta | \mathbf{y}) \frac{\hat{p}^r(\theta)}{p(\theta)}$. Greenberg et al. [2019] overcome this by deriving the new objective $\mathbb{E}_{\mathcal{D}} \left[\frac{1}{Z} q_f(\theta | \mathbf{y}) \frac{\hat{p}^r(\theta)}{p(\theta)} \right]$ which however requires the computation of a normalization constant Z . Durkan et al. [2020] show that APT is equivalent to methods that learn the likelihood-to-evidence ratio $r(\mathbf{y}, \theta) = \frac{p(\mathbf{y} | \theta)}{p(\mathbf{y})}$ and then build a surrogate posterior $\hat{p}(\theta | \mathbf{y}) \propto \hat{r}(\mathbf{y}, \theta) p(\theta)$.

APT can simulate posterior realizations by sampling from the normalizing flow base distribution first, and then propagating the samples through the flow layers. This can lead to posteriors that are outside of the prior bounds which need to be rejected and the procedure repeated until a sample of desired size has been taken. Specifically, if the prior distributions are constrained, e.g., containing scale parameters, or are very narrow, APT is known to exert ‘leakage’, i.e., the posterior approximation might produce samples that are not within the prior bounds. In this case, the rejection rate of posterior samples is elevated, for instance, as reported in Durkan et al. [2020] or Glöckler et al. [2022], the latter of which having observed rejection rates of up to 99%, which necessitates the use of MCMC methods instead. Leakage significantly reduces the usefulness of SNPE methods in comparison to SNL where draws are generated using MCMC in the first place. Furthermore, for structured data sets, e.g., time series data, APT requires facilitating a second neural network to embed the data before conditioning which increases the number of effective parameters.

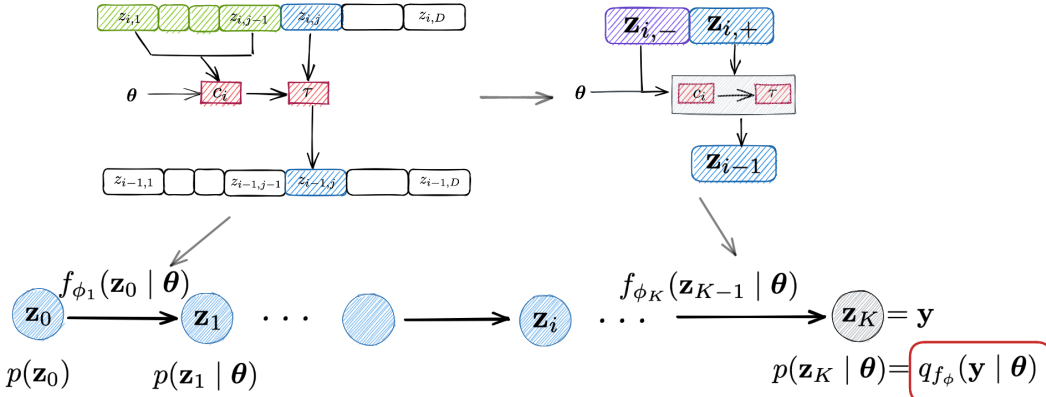


Figure 1: **Surjective sequential neural likelihood.** SSNL fits a surrogate model to approximate the likelihood function in a Bayesian generative model (bottom). The underlying flow consists of both dimensionality-preserving bijective layers (top-left) and dimensionality-reducing surjective layers (top-right) which use bijections on a subset of a data vector. Through dimensionality reduction, we achieve more competitive likelihood estimation than the vanilla SNL method.

3 Surjective sequential neural likelihood estimation

Our new method, *Surjective Sequential Neural Likelihood* (SSNL) estimation, iteratively fits a surjective normalizing flow as a surrogate model for the intractable likelihood function and then builds a proposal posterior distribution using this approximation (Algorithm 1). We hypothesize that if the data lie in a high-dimensional ambient space, embedding the data in a lower-dimensional space should improve likelihood estimation. We model the surrogate likelihood $q_f(\mathbf{y} | \theta)$ as a combination of K conditional dimensionality-preserving and dimensionality-reducing normalizing flows. For ease of notation, we drop sub- and superscripts wherever it does not decrease readability.

Specifically, we model the dimensionality-reducing transformations using surjective normalizing flows [Nielsen et al., 2020, Klein et al., 2021] by defining the pullback only on a subset of the data vector $\mathbf{y} \in \mathbb{R}^P$:

$$\mathbf{z} = f^{-1}(\mathbf{y}_{1:Q}) \quad (2)$$

and we define the respective the forward transformation generatively as

$$\mathbf{y} = \begin{bmatrix} \mathbf{y}_{1:Q} = f(\mathbf{z}) \\ \mathbf{y}_{Q+1:P} \sim p(\mathbf{y}_{Q+1:P} \mid \mathbf{z}) \end{bmatrix} \quad (3)$$

with $Q < P$ and $\mathbf{z} \in \mathbb{R}^Q$. Concretely, for any inverse transformation f^{-1} , we split $\mathbf{y} = [\mathbf{y}_-, \mathbf{y}_+]^T$ into two sub-vectors of not necessarily equal length and then define the inverse mapping as $f_{\theta, \mathbf{y}_-}^{-1}(\mathbf{y}_+)$ as a conditional autoregressive flow (i.e, conditional on the concatenation of the vectors θ and \mathbf{y}_-) and $p(\mathbf{y}_- \mid f_{\theta, \mathbf{y}_-}^{-1}(\mathbf{y}_+))$ as a conditional density (that might be in turn parameterized by a neural network). For a surjective normalizing flow, the likelihood contribution consequently becomes the product of the Jacobian determinant of the transformation acting on \mathbf{y}_+ and the conditional probability $p(\mathbf{y}_- \mid f_{\theta, \mathbf{y}_-}^{-1}(\mathbf{y}_+))$, such that for a surjective flow with only a single transformation the probability of an observation is computed as

$$q_f(\mathbf{y} \mid \theta) = p(\mathbf{z}_0) p(\mathbf{y}_- \mid \mathbf{z}_0) \left| \det J \right|^{-1} \quad (4)$$

where $\mathbf{z}_0 = f_{\theta, \mathbf{y}_-}^{-1}(\mathbf{y}_+)$, $\det J = \det \frac{\partial f_{\theta, \mathbf{y}_-}}{\partial \mathbf{z}_0}$ is again the Jacobian determinant of the forward transformation acting on the low-dimensional vector $\mathbf{z}_0 \in \mathbb{R}^Q$. Analogously to bijective flows, the conditional density of a normalizing flow that consists of K dimensionality-reducing layers has the following form:

$$q_f(\mathbf{y} \mid \theta) = p(\mathbf{z}_0) \prod_{k=1}^K p(\mathbf{z}_{k,-} \mid f_{\theta, \mathbf{z}_{k,-}}^{-1}(\mathbf{z}_{k,+})) \left| \det J_k \right|^{-1} \quad (5)$$

where $J_k = \frac{\partial f_{\theta, \mathbf{z}_{k,-}}}{\partial \mathbf{z}_{k-1,+}}$ is the Jacobian of the k th transformation f_k and where we for readability slightly abused notation denoting with $f_{\theta, \mathbf{z}_{k,-}}$ the transformation f_k that uses the concatenation of θ and $\mathbf{z}_{k,-}$ for conditioning.

SSNL models the likelihood used for simulation-based-inference as a composition of dimensionality-preserving and -reducing layers:

$$q_f(\mathbf{y} \mid \theta) = p(\mathbf{z}_0) \prod_{k \in \mathcal{K}_{\text{pres}}} \left| \det J_k \right|^{-1} \prod_{k \in \mathcal{K}_{\text{red}}} p(\mathbf{z}_{k,-} \mid f_{\theta, \mathbf{z}_{k,-}}^{-1}(\mathbf{z}_{k,+})) \left| \det J_k \right|^{-1} \quad (6)$$

where $\mathcal{K}_{\text{pres}}$ and \mathcal{K}_{red} represent sets of indexes for dimensionality-preserving and -reducing flow layers, respectively. For instance, for a total of $K = 5$ normalizing flow layers, one could alternate between bijections and surjections by setting the sets $\mathcal{K}_{\text{pres}} = \{1, 3, 5\}$ and $\mathcal{K}_{\text{red}} = \{2, 4\}$. As mentioned before, we commonly parameterize f using MAFs, but in practice also masked coupling flows [Dinh et al., 2015, 2017] with arbitrary conditioners are possible and in fact in certain scenarios more reasonable since they allow for more flexible conditioning networks ϕ_k .

The lower-dimensional embedding of SSNL solves previous issues of SNL as pointed out in Greenberg et al. [2019], for instance, when observations consist of uninformative data dimensions or when the data lie along a lower-dimensional manifold embedded in a high dimensional space. In addition, through the dimensionality-reduction the flows require less parameters in general which empirically speeds up computation such that more of the computational budget can be used for the simulator.

The dimensionality-reducing flow is fully deterministic in the pullback direction, i.e., in the case of likelihood estimation, but requires sampling from the conditional $p(\mathbf{z}_- \mid f_{\theta, \mathbf{z}_-}^{-1}(\mathbf{z}_+))$ during the forward transformation and, hence, has additional stochastic components other than the base distribution $p(\mathbf{z}_0)$. For our setting, i.e., density estimation, this is however not a limitation.

Similarly to APT and SNL, SSNL is trained in R rounds where in every round a new proposal posterior is defined. The proposal posterior can be either sampled from using MCMC methods or approximated with another conditional distribution using variational inference (Algorithm 1). A complete derivation of the dimensionality-reducing layer can be found in Appendix A.

Algorithm 1: Surjective sequential neural likelihood

Inputs: observation \mathbf{y}_0 , prior distribution $p(\theta)$, surjective normalizing flow $q_f(\mathbf{y} \mid \theta)$, simulations per round N , number of rounds R
Outputs: approximate posterior distribution $\hat{p}^R(\theta \mid \mathbf{y}_0)$
Initialize: proposal $\hat{p}^0(\theta \mid \mathbf{y}_0) \leftarrow p(\theta)$, data set $\mathcal{D} = \{\}$
for $r \leftarrow 1, \dots, R$ **do**
 for $n \leftarrow 1, \dots, N$ **do**
 sample $\theta_n \sim \hat{p}^{r-1}(\theta \mid \mathbf{y}_0)$
 simulate $\mathbf{y}_n \leftarrow \text{sim}(\theta_n)$ using the simulator function
 concatenate $\mathcal{D} \leftarrow \{\mathcal{D}, (\mathbf{y}_n, \theta_n)\}$
 end
 train $q_f(\mathbf{y} \mid \theta)$ on \mathcal{D}
 set $\hat{p}^r(\theta \mid \mathbf{y}_0) \propto q_f(\mathbf{y}_0 \mid \theta)p(\theta)$
end

4 Experiments

We compare SSNL to SNL and APT on several synthetic and real-world experiments to highlight the advantages and disadvantages of the method. We follow the experimental setup of Papamakarios et al. [2019] and Greenberg et al. [2019] as closely as possible. We parameterize the normalizing flows of each method with the same number of layers per experiment, which depending on the experiment is between five and ten. Each flow layer is parameterised with a two-layer neural network consisting of 50 neurons per layer. We use tanh activation functions throughout the experiments. All networks are trained using Adam [Kingma and Ba, 2015] with a fixed learning rate of 0.0001 and a mini-batch size of 100, and we run the optimizer until no improvement on a validation set can be observed. We deliberately did not do any hyper-parameter or architecture optimization, but followed previous approaches and set the number of layers somewhat arbitrarily depending on data dimensionality to achieve an unbiased performance estimate.

For SSNL and SNL experiments, we developed two Python packages called `sbi.jax` and `surjectors` which use JAX for gradient computations [Bradbury et al., 2018] and TensorFlow Probability [Dillon et al., 2017] for MCMC sampling. We use slice sampling [Neal, 2003, Bélisle et al., 1993] to sample from the intermediate and final posterior distributions $p^r(\theta \mid \mathbf{y}_0)$ using 4 chains of a fixed length of 10 000 each of which the first 5 000 iterations are discarded as warm-up. For SNPE experiments, we use the SBI toolbox of Tejero-Cantero et al. [2020]. For experiments for which the un-normalized posterior is available and can be sampled from, we compute the maximum mean discrepancy (MMD; Gretton et al. [2012], Lueckmann et al. [2021]) between true posterior and approximate posterior, otherwise we compute the mean squared error between the approximate posterior and the prior parameters that were used to simulate \mathbf{y}_0 . Convergence of the true posteriors in this case has been diagnosed using the potential scale reduction factor [Gelman and Rubin, 1992], effective sample size calculations, and conventional graphical diagnostics [Gabry et al., 2019].

Each experiment was run on a single virtual machine equipped with a Tesla P100 GPU with 12GB of memory and took depending on complexity of the experiment and model between two hours to two days to finish. We found that our JAX-based implementations of SSNL and SNL and sampling using the slice sampler of Tensorflow Probability was significantly faster than the MCMC or rejection samplers of the SBI toolbox. Hence, not all experiments finished until the submission deadline and have not yet been replicated multiple times (more results in Appendix B). The full details for each

experiment can be found in Appendix B. Code that reproduces the experiments with user instructions can be found in Appendix C or GitHub at <https://github.com/dirmeyer/ssnl>.

Simple likelihood complex posterior Following Papamakarios et al. [2019] and Greenberg et al. [2019], we conduct experiments on a model with a simple likelihood but complex posterior geometry:

$$\begin{aligned}
\theta_i &\sim \text{Uniform}(-3, 3) \text{ for } i = 1, \dots, 5 \\
\mu(\boldsymbol{\theta}) &= (\theta_1, \theta_2), \phi_1 = \theta_3^2, \phi_2 = \theta_4^2 \\
\Sigma(\boldsymbol{\theta}) &= \begin{pmatrix} \phi_1^2 & \tanh(\theta_5)\phi_1\phi_2 \\ \tanh(\theta_5)\phi_1\phi_2 & \phi_2^2 \end{pmatrix} \\
\mathbf{y}_j \mid \boldsymbol{\theta} &\sim \mathcal{N}(\mathbf{y}_j; \mu(\boldsymbol{\theta}), \Sigma(\boldsymbol{\theta})) \text{ for } j = 1, \dots, 4 \\
\mathbf{y} &= [\mathbf{y}_1, \dots, \mathbf{y}_4]^T
\end{aligned} \tag{7}$$

We use the same observation \mathbf{y}_0 as in Papamakarios et al. [2019]. Inference in this experiments can be done exactly using MCMC (up to some MC error). Here, with a sufficient number of rounds R and data simulations N , SSNL should not necessarily outperform SNL, because the latent variables $\boldsymbol{\theta}$ and the data dimensionality are roughly the same and neither of the latter methods should have problems inferring the parameters (Figure 4 first column). Interestingly, SSNL still has a performance advantage over SNL and APT.

As Greenberg et al. [2019] report, the performance of SNL degrades if the data contain non-informative data dimensions, or generally, if the data lies along a lower-dimensional manifold. To show that SSNL does not have the same drawback, we conduct experiments where we add 42 and 492 non-informative data dimensions sampled from a standard multivariate Gaussian to the original data, i.e., we sample additional $\mathbf{y}_j \sim \mathcal{N}_2(\mathbf{0}, \mathbf{I})$ and appended them to the data of Equation 7. In each of these experiments, SSNL has a performance advantage over the other two methods (Figure 4 second and third columns). We observed that the training of SSNL converges faster than the other two methods, allowing for an increased computational budget for the simulator which could be relevant for compute-intensive experiments.

Solar Dynamo We applied SSNL, SNL and APT to a real-world solar dynamo model from the solar physics literature that models the magnetic field strength of the sun (see, e.g., Charbonneau et al. [2005] and references therein). The model is a non-linear time series model with both additive and multiplicative noise terms

$$\begin{aligned}
g(y) &= \frac{1}{2}[1 + \text{erf}(\frac{y-b_1}{w_1})][1 - \text{erf}(\frac{y-b_2}{w_2})] \\
y_{i+1} &\leftarrow \alpha_i g(y_i) y_i + \epsilon_i, \quad \alpha_i \sim \text{Unif}(\alpha, \alpha + \delta), \quad \epsilon_i \sim \text{Unif}[0, \epsilon] \quad \forall i = 0, \dots, N
\end{aligned}$$

that has three random latent parameters $\boldsymbol{\theta} = [\alpha, \delta, \epsilon]^T$. The model is interesting, because it has more noise components than observed outcomes and integrating out the noise components yields a marginal likelihood that is outside the exponential family. Consequently, the number of sufficient statistics for such a model is unbounded (with the sample size N) according to Pitman-Koopman-Darmois theorem. We choose initial parameters as in Albert et al. [2022] and simulate a single time series of length $N = 200$ (see Appendix B for details). SSNL has an advantage over both SNL and APT for this experiment (measured by the mean squared error w.r.t. the prior parameter values; see Figure 4 last column). Having a closer look at the posterior distributions after the final round (Figure 3), one can observe that, e.g., the posterior means for the parameter α for SNL and APT have a larger bias than for SSNL, and that SSNL generally manages to put more mass on the correct regions of the posterior. Interestingly, APT already after the first iteration produces convincing posterior inferences (see Figure 4 last column). Presumably this due to the fact, that likelihood-based methods need more observations for fitting the time series data while APT can model the low-dimensional posterior directly.

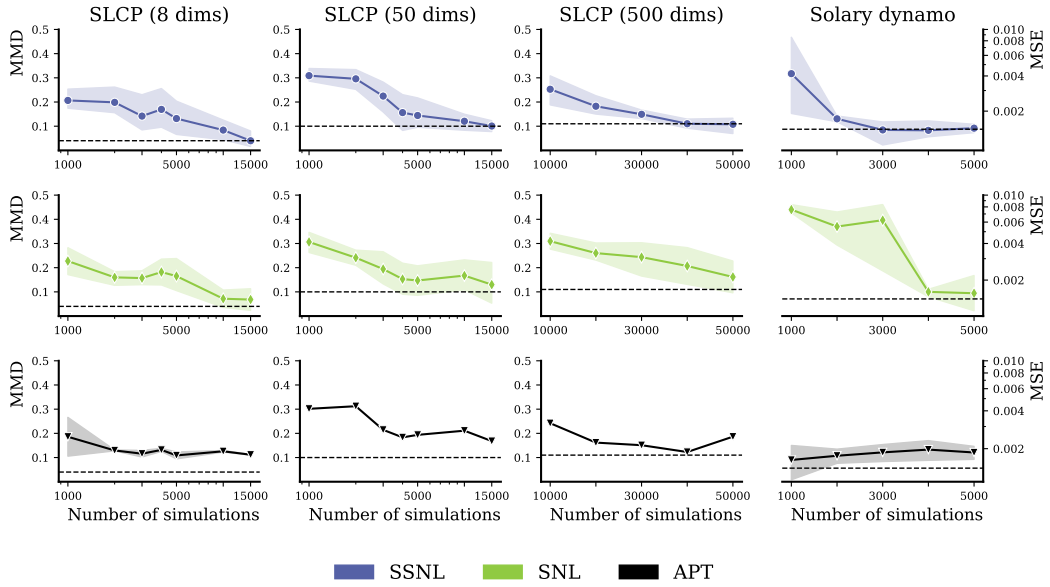


Figure 2: **Experimental results.** The left three columns show the benchmarks on a data set with simple likelihood and complex posterior geometry. SSNL generally outperforms SNL and APT (distance measured using MMD, lower is better). Right column: we applied the three methods also to a solar dynamo model where SSNL has a performance advantage over the other methods with increased number of simulations (distance measured using MSE, note the log-scale on the y-axis). Horizontal lines on all plots show the lowest MMD or MSE per experiment.

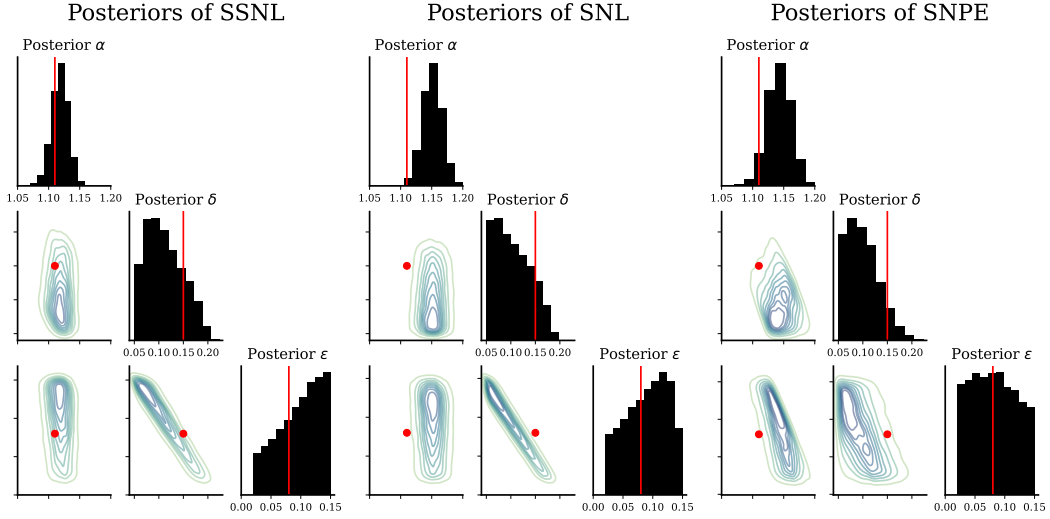


Figure 3: **Posterior distributions of a solar dynamo model.** Figures on the diagonal show the marginal distributions of each parameter, while the figures on the off-diagonal represent two-dimensional kernel density estimates. SSNL manages to put the most mass on the correct regions of the posterior while both SNL and SNPE are exerting a higher bias.

5 Discussion

We introduced *Surjective Sequential Neural Likelihood* estimation, a new method for approximate Bayesian inference for models with intractable likelihood function. In comparison to SNL which uses bijective normalizing flows, our method uses a composition of dimensionality-reducing surjections and dimensionality-preserving bijections to approximate the likelihood function. Especially when simulators produce high-dimensional data samples that can be embedded in a low dimensional space, we showed that our method performs favourably in contrast to SNL and APT thereby tackling an important short-coming of likelihood-based SBI methods.

We anticipate that our method will complement other approaches to simulation-based inference well, but do not argue that it should be generally preferred over others. For instance, if appropriate summary statistics exist and a sufficient simulation budget is available, SMC-ABC methods are still valid alternatives to approaches utilizing neural density estimation. Likewise, methods that target the posterior directly, e.g., APT, are in certain scenarios preferable over likelihood-based methods, for instance, when prior distributions are unconstrained and the likelihood function is potentially difficult to model. In scenarios, where prior distributions are bounded or narrow, or the default rejection sampling procedure of SNPE methods yields elevated rejection rates, or the data is embedded in a low-dimensional manifold, SSNL will likely outperform SNL and APT. Consequently, the method of choice depends on the problem at hand.

The literature has established several attractive approaches to simulation-based inference. However, to the best of our knowledge up until now most experiments have been using simple toy models to demonstrate the methodology, e.g., with low-dimensional parameter spaces, whereas systematic validations on more difficult real-world use cases or situations where the simulator is miss-specified have not been conducted. In a similar line of research, Hermans et al. [2022] report that neural network based SBI methods such as SNL can be overconfident in approximating the posterior which makes the inferences unreliable in practice and useless for scientific inquiries. While we did not conduct experiments specifically to address this issue, it might be interesting to evaluate to what extent dimensionality-reducing flows might yield more robust parameter inferences for these scenarios.

Acknowledgments and Disclosure of Funding

This research was supported by the Swiss National Science Foundation (Grant No. 200021_208249).

References

Carlo Albert, Hans R Künsch, and Andreas Scheidegger. A simulated annealing approach to approximate Bayes computations. *Statistics and Computing*, 25:1217–1232, 2015.

Carlo Albert, Simone Ulzega, Firat Ozdemir, Fernando Perez-Cruz, and Antonietta Mira. Learning summary statistics for Bayesian inference with autoencoders. *SciPost Physics Core*, 5(3):043, 2022.

Igor Babuschkin, Baumli, et al. The DeepMind JAX Ecosystem, 2020. URL <http://github.com/deepmind>.

Mark A Beaumont, Jean-Marie Cornuet, Jean-Michel Marin, and Christian P Robert. Adaptive approximate Bayesian computation. *Biometrika*, 96(4):983–990, 2009.

Claude JP Bélisle, H Edwin Romeijn, and Robert L Smith. Hit-and-run algorithms for generating multivariate distributions. *Mathematics of Operations Research*, 18(2):255–266, 1993.

James Bradbury, Roy Frostig, Peter Hawkins, Matthew James Johnson, Chris Leary, Dougal Maclaurin, George Necula, Adam Paszke, Jake VanderPlas, Skye Wanderman-Milne, and Qiao Zhang. JAX: composable transformations of Python+NumPy programs, 2018. URL <http://github.com/google/jax>.

Johann Brehmer. Simulation-based inference in particle physics. *Nature Reviews Physics*, 3(5):305–305, 2021.

Johann Brehmer, Kyle Cranmer, Gilles Louppe, and Juan Pavez. Constraining effective field theories with machine learning. *Phys. Rev. Lett.*, 121:111801, 2018.

Steve Brooks, Andrew Gelman, Galin Jones, and Xiao-Li Meng. *Handbook of Markov Chain Monte Carlo*. CRC press, 2011.

Paul Charbonneau, Cédric St-Jean, and Pia Zacharias. Fluctuations in babcock-leighton dynamos. i. period doubling and transition to chaos. *The Astrophysical Journal*, 619(1):613, 2005.

Kyle Cranmer, Juan Pavez, and Gilles Louppe. Approximating likelihood ratios with calibrated discriminative classifiers. *arXiv preprint arXiv:1506.02169*, 2015.

Kyle Cranmer, Johann Brehmer, and Gilles Louppe. The frontier of simulation-based inference. *Proceedings of the National Academy of Sciences*, 117(48):30055–30062, 2020.

Edmond Cunningham, Renos Zabounidis, Abhinav Agrawal, Madalina Fiterau, and Daniel Sheldon. Normalizing flows across dimensions. In *ICML Workshop on Theoretical Foundations and Applications of Deep Generative Models*, 2020.

Biwei Dai and Uros Seljak. Sliced iterative normalizing flows. In *ICML Workshop on Invertible Neural Networks, Normalizing Flows, and Explicit Likelihood Models*, 2021.

Maximilian Dax, Stephen R. Green, Jonathan Gair, Jakob H. Macke, Alessandra Buonanno, and Bernhard Schölkopf. Real-time gravitational wave science with neural posterior estimation. *Phys. Rev. Lett.*, 127:241103, 2021.

Michael Deistler, Pedro J. Goncalves, and Jakob H. Macke. Truncated proposals for scalable and hassle-free simulation-based inference. In *Advances in Neural Information Processing Systems*, 2022.

Pierre Del Moral, Arnaud Doucet, and Ajay Jasra. An adaptive sequential Monte Carlo method for approximate Bayesian computation. *Statistics and Computing*, 22:1009–1020, 2012.

Arnaud Delaunoy, Antoine Wehenkel, Tanja Hinderer, Samaya Nissanke, Christoph Weniger, Andrew R Williamson, and Gilles Louppe. Lightning-fast gravitational wave parameter inference through neural amortization. In *Workshop on Machine Learning and the Physical Sciences, Advances in Neural Information Processing Systems*, 2020.

Joshua V Dillon, Ian Langmore, Dustin Tran, Eugene Brevdo, Srinivas Vasudevan, Dave Moore, Brian Patton, Alex Alemi, Matt Hoffman, and Rif A Saurous. Tensorflow distributions. *arXiv preprint arXiv:1711.10604*, 2017.

Laurent Dinh, David Krueger, and Yoshua Bengio. NICE: non-linear independent components estimation. In *Workshop Track, International Conference on Learning Representations*, 2015.

Laurent Dinh, Jascha Sohl-Dickstein, and Samy Bengio. Density estimation using real NVP. In *International Conference on Learning Representations*, 2017.

Conor Durkan, Artur Bekasov, Iain Murray, and George Papamakarios. Neural spline flows. In *Advances in Neural Information Processing Systems*, 2019.

Conor Durkan, Iain Murray, and George Papamakarios. On contrastive learning for likelihood-free inference. In *Proceedings of the 37th International Conference on Machine Learning*, 2020.

Charles Fefferman, Sanjoy Mitter, and Hariharan Narayanan. Testing the manifold hypothesis. *Journal of the American Mathematical Society*, 29(4):983–1049, 2016.

Jonah Gabry, Daniel Simpson, Aki Vehtari, Michael Betancourt, and Andrew Gelman. Visualization in bayesian workflow. *Journal of the Royal Statistical Society Series A: Statistics in Society*, 182(2):389–402, 2019.

Andrew Gelman and Donald B. Rubin. Inference from iterative simulation using multiple sequences. *Statistical Science*, 7(4):457 – 472, 1992.

Mathieu Germain, Karol Gregor, Iain Murray, and Hugo Larochelle. Made: Masked autoencoder for distribution estimation. In *Proceedings of the 32nd International Conference on Machine Learning*, 2015.

Manuel Glöckler, Michael Deistler, and Jakob H. Macke. Variational methods for simulation-based inference. In *International Conference on Learning Representations*, 2022.

David Greenberg, Marcel Nonnenmacher, and Jakob Macke. Automatic posterior transformation for likelihood-free inference. In *Proceedings of the 36th International Conference on Machine Learning*, 2019.

Arthur Gretton, Karsten M Borgwardt, Malte J Rasch, Bernhard Schölkopf, and Alexander Smola. A kernel two-sample test. *The Journal of Machine Learning Research*, 13(1):723–773, 2012.

Joeri Hermans, Nilanjan Banik, Christoph Weniger, Gianfranco Bertone, and Gilles Louppe. Towards constraining warm dark matter with stellar streams through neural simulation-based inference. *Monthly Notices of the Royal Astronomical Society*, 507(2).

Joeri Hermans, Volodimir Begy, and Gilles Louppe. Likelihood-free MCMC with amortized approximate ratio estimators. In *Proceedings of the 37th International Conference on Machine Learning*, 2020.

Joeri Hermans, Arnaud Delaunoy, François Rozet, Antoine Wehenkel, Volodimir Begy, and Gilles Louppe. A crisis in simulation-based inference? Beware, your posterior approximations can be unfaithful. *Transactions on Machine Learning Research*, 2022.

Diederik P. Kingma and Jimmy Ba. Adam: A method for stochastic optimization. In *International Conference on Learning Representations*, 2015.

Samuel Klein, John A. Raine, Sebastian Pina-Otey, Slava Voloshynovskiy, and Tobias Golling. Funnels: Exact maximum likelihood with dimensionality reduction. In *Workshop on Bayesian Deep Learning, Advances in Neural Information Processing Systems*, 2021.

Jan-Matthis Lueckmann, Pedro J Goncalves, Giacomo Bassetto, Kaan Öcal, Marcel Nonnenmacher, and Jakob H Macke. Flexible statistical inference for mechanistic models of neural dynamics. In *Advances in Neural Information Processing Systems*, 2017.

Jan-Matthis Lueckmann, Jan Boelts, David Greenberg, Pedro Goncalves, and Jakob Macke. Benchmarking simulation-based inference. In *Proceedings of the 24th International Conference on Artificial Intelligence and Statistics*, 2021.

Benjamin Kurt Miller, Christoph Weniger, and Patrick Forré. Contrastive neural ratio estimation. In *Advances in Neural Information Processing Systems*, 2022.

Radford M Neal. Slice sampling. *The Annals of Statistics*, 31(3):705–767, 2003.

Didrik Nielsen, Priyank Jaini, Emiel Hoogeboom, Ole Winther, and Max Welling. Survae flows: Surjections to bridge the gap between vaes and flows. *Advances in Neural Information Processing Systems*, 2020.

George Papamakarios and Iain Murray. Fast ε -free inference of simulation models with Bayesian conditional density estimation. In *Advances in Neural Information Processing Systems*, volume 29, 2016.

George Papamakarios, Theo Pavlakou, and Iain Murray. Masked autoregressive flow for density estimation. In *Advances in Neural Information Processing Systems*, 2017.

George Papamakarios, David Sterratt, and Iain Murray. Sequential neural likelihood: Fast likelihood-free inference with autoregressive flows. In *Proceedings of the 22nd International Conference on Artificial Intelligence and Statistics*, 2019.

George Papamakarios, Eric Nalisnick, Danilo Jimenez Rezende, Shakir Mohamed, and Balaji Lakshminarayanan. Normalizing flows for probabilistic modeling and inference. *The Journal of Machine Learning Research*, 22(1):2617–2680, 2021.

Jonathan K Pritchard, Mark T Seielstad, Anna Perez-Lezaun, and Marcus W Feldman. Population growth of human y chromosomes: a study of y chromosome microsatellites. *Molecular Biology and Evolution*, 16(12):1791–1798, 1999.

Oliver Ratmann, Ole Jørgensen, Trevor Hinkley, Michael Stumpf, Sylvia Richardson, and Carsten Wiuf. Using likelihood-free inference to compare evolutionary dynamics of the protein networks of *H. pylori* and *P. falciparum*. *PLoS Computational Biology*, 3(11):e230, 2007.

Scott A Sisson, Yanan Fan, and Mark Beaumont. *Handbook of Approximate Bayesian Computation*. CRC Press, 2018.

Alvaro Tejero-Cantero, Jan Boelts, Michael Deistler, Jan-Matthis Lueckmann, Conor Durkan, Pedro J. Gonçalves, David S. Greenberg, and Jakob H. Macke. sbi: A toolkit for simulation-based inference. *Journal of Open Source Software*, 5(52):2505, 2020.

Owen Thomas, Ritabrata Dutta, Jukka Corander, Samuel Kaski, and Michael U Gutmann. Likelihood-free inference by ratio estimation. *Bayesian Analysis*, 17(1):1–31, 2022.

Martin J. Wainwright and Michael I. Jordan. Graphical models, exponential families, and variational inference. *Foundations and Trends in Machine Learning*, 1(1–2):1–305, 2008.

Samuel Wiqvist, Jes Frellsen, and Umberto Picchini. Sequential neural posterior and likelihood approximation. *arXiv preprint arXiv:2102.06522*, 2021.

Appendix A Derivation surjection layer

The derivation of the surjection layer used in SSNL largely follows the SurVAE framework of Nielsen et al. [2020] and Klein et al. [2021]. The SurVAE framework models the log-probability $\log p(\mathbf{y})$ of a P -dimensional data point $\mathbf{y} \in \mathcal{Y}$ as

$$\log p(\mathbf{y}) = \log p(\mathbf{z}) + V(\mathbf{y}, \mathbf{z}) + E(\mathbf{y}, \mathbf{z}), \quad \mathbf{z} \sim q(\mathbf{z} \mid \mathbf{y}) \quad (8)$$

where $q(\mathbf{z} \mid \mathbf{y})$ is some amortized (variational) distribution, $\mathbf{z} \in \mathcal{Z}$ is a latent variable with distribution $p(\mathbf{z})$, $V(\mathbf{y}, \mathbf{z})$ is denoted likelihood contribution term and $E(\mathbf{y}, \mathbf{z})$ is a bound looseness term.

Nielsen et al. [2020] define the likelihood contribution for inference surjections as

$$V(\mathbf{y}, \mathbf{z}) = \lim_{q(\mathbf{z} \mid \mathbf{y}) \rightarrow \delta(\mathbf{z} - h^{-1}(\mathbf{y}))} \mathbb{E}_{q(\mathbf{z} \mid \mathbf{y})} \left[\log \frac{p(\mathbf{y} \mid \mathbf{z})}{q(\mathbf{z} \mid \mathbf{y})} \right] \quad (9)$$

where $p(\mathbf{y} \mid \mathbf{z})$ is some generative stochastic transformation, $h^{-1} : \mathcal{Y} \rightarrow \mathcal{Z}$ is an inference surjection and where we for convenience of notation denote with $h : \mathcal{Z} \rightarrow \mathcal{Y}$ a right inverse function to h^{-1} . For bijective normalizing flows the bound looseness term equals $E(\mathbf{y}, \mathbf{z}) = 0$. For surjective normalizing flows, the same is true if a right inverse h exists (i.e., when the stochastic right inverse condition is satisfied).

By observing (see also Appendix A of Nielsen et al. [2020] and main manuscript Klein et al. [2021]) that the composition of a differentiable function g with a Dirac δ function and a bijection f is

$$\int \delta(g(\mathbf{y})) f(g(\mathbf{y})) \left| \det \frac{\partial g(\mathbf{y})}{\partial \mathbf{y}} \right| d\mathbf{y} = \int \delta(\mathbf{u}) f(\mathbf{u}) d\mathbf{u} \quad (10)$$

we can conclude that

$$\delta(g(\mathbf{y})) = \delta(\mathbf{y} - \mathbf{y}_0) \left| \det \frac{\partial g(\mathbf{y})}{\partial \mathbf{y}} \right|_{\mathbf{y}=\mathbf{y}_0}^{-1} \quad (11)$$

where \mathbf{y}_0 is the root of g (which assumes that f has compact support, the root is unique and that the Jacobian is not singular).

We now define a conditional bijection $f_{\mathbf{y}_{1:Q}}(\mathbf{z})$ and its inverse $f_{\mathbf{y}_{1:Q}}^{-1}(\mathbf{y}_{Q+1:P})$ for any $Q < P$, set $g(\mathbf{y}) = \mathbf{z} - f_{\mathbf{y}_{1:Q}}^{-1}(\mathbf{y}_{Q+1:P})$ (which has its root at $\mathbf{y}_0 = f_{\mathbf{y}_{1:Q}}(\mathbf{z})$) and define

$$q(\mathbf{z} \mid \mathbf{y}) = \delta \left(\mathbf{z} - f_{\mathbf{y}_{1:Q}}^{-1}(\mathbf{y}_{Q+1:P}) \right) \quad (12)$$

$$= \delta \left(\mathbf{y}_{Q+1:P} - f_{\mathbf{y}_{1:Q}}(\mathbf{z}) \right) \left| \det J^{-1} \right|^{-1} \quad (13)$$

$$(14)$$

where

$$J^{-1} = \frac{\partial f_{\mathbf{y}_{1:Q}}^{-1}(\mathbf{y}_{Q+1:P})}{\partial \mathbf{y}_{Q+1:P}} \Big|_{\mathbf{y}_{Q+1:P} = f_{\mathbf{y}_{1:Q}}(\mathbf{z})} \quad (15)$$

Using this result and the conditional distribution $p(\mathbf{y} \mid \mathbf{z}) = p(\mathbf{y}_{1:Q} \mid \mathbf{z})$ the likelihood contribution for a surjection layer becomes

$$V(\mathbf{y}, \mathbf{z}) = \lim_{q(\mathbf{z}|\mathbf{y}) \rightarrow \delta(\mathbf{z}-h^{-1}(\mathbf{y}))} \mathbb{E}_{q(\mathbf{z}|\mathbf{y})} \left[\log \frac{p(\mathbf{y}|\mathbf{z})}{q(\mathbf{z}|\mathbf{y})} \right] \quad (16)$$

$$= \int \delta(\mathbf{z} - f_{\mathbf{y}_{1:Q}}^{-1}(\mathbf{y}_{Q+1:P})) \log \frac{p(\mathbf{y}_{1:Q}|\mathbf{z})}{\delta(\mathbf{z} - f_{\mathbf{y}_{1:Q}}^{-1}(\mathbf{y}_{Q+1:P}))} d\mathbf{z} \quad (17)$$

$$= \log p(\mathbf{y}_{1:Q} | f_{\mathbf{y}_{1:Q}}^{-1}(\mathbf{y}_{Q+1:P})) - \log \left| \det J^{-1} \right|^{-1} \quad (18)$$

$$= \log p(\mathbf{y}_{1:Q} | f_{\mathbf{y}_{1:Q}}^{-1}(\mathbf{y}_{Q+1:P})) + \log \left| \det J^{-1} \right| \quad (19)$$

Appendix B Experimental details

B.1 Training

We trained each model using an Adam optimizer with fixed learning rate of $r = 0.0001$ and momentums $b_1 = 0.9$ and $b_2 = 0.999$ using the optimization framework Optax [Babuschkin et al., 2020] for the implementations of SSNL and SNL, and the implementation of the SBI toolbox for APT [Tejero-Cantero et al., 2020]. Each experiment uses a mini-batch size of 100. The optimizer is run until a maximum of 1000 epochs is reached or no improvement on a validation set can be observed for 10 consecutive iterations. The validation set consists of 10% of the entire data set, while the other 90% are used for training. For each round, we start training the neural network from scratch and do not continue from the previously learned state.

For SSNL and SNL, we use the slice sampler [Neal, 2003] from TensorFlow Probability [Dillon et al., 2017] to sample from the intermediate and final posterior distributions $p^r(\boldsymbol{\theta} | \mathbf{y}_0)$ using 4 chains of a fixed length of 10 000 each of which the first 5 000 iterations are discarded as warm-up. For SNPE experiments, we use the SBI toolbox of Tejero-Cantero et al. [2020] for sampling.

Generally, we did not conduct hyperparameter optimization for any model, nor did we optimize on the MAF architecture or number of layers, but followed the experimental details of Papamakarios et al. [2019], Greenberg et al. [2019] as much as possible and somewhat arbitrarily selected number of layers, etc. for the different models.

For versioning details, see the conda environment files in Appendix C.

B.2 Simple likelihood complex posterior geometry

B.2.1 SLCP with eight dimensions

The SLCP model with 8 dimensions uses the following generative process

$$\begin{aligned} \theta_i &\sim \text{Uniform}(-3, 3) \text{ for } i = 1, \dots, 5 \\ \boldsymbol{\mu}(\boldsymbol{\theta}) &= (\theta_1, \theta_2), \phi_1 = \theta_3^2, \phi_2 = \theta_4^2 \\ \boldsymbol{\Sigma}(\boldsymbol{\theta}) &= \begin{pmatrix} \phi_1^2 & \tanh(\theta_5)\phi_1\phi_2 \\ \tanh(\theta_5)\phi_1\phi_2 & \phi_2^2 \end{pmatrix} \\ \mathbf{y}_j | \boldsymbol{\theta} &\sim \mathcal{N}(\mathbf{y}_j; \boldsymbol{\mu}(\boldsymbol{\theta}), \boldsymbol{\Sigma}(\boldsymbol{\theta})) \text{ for } j = 1, \dots, 4 \\ \mathbf{y} &= [\mathbf{y}_1, \dots, \mathbf{y}_4]^T \end{aligned} \quad (20)$$

SLCP with eight dimensions has been trained in $R = 15$ rounds. Each round $N = 1000$ samples are drawn from the proposal. We used the same random seeds for each model and iteration using the random number generator of JAX [Bradbury et al., 2018] on the same hardware to guarantee identical training and validation data.

SSNL The SSNL architecture uses a total of $K = 5$ layers, the third of which is a surjection layer with a reduction factor of 25%, i.e., we randomly take 75% of the number elements of the previous

layers and use this number as new latent dimension. Each of the layers is parameterized by a MAF which uses a MADE network with 2 layers with 50 neurons each as conditioner.

SNL and APT SNL/APT use a MAF with $K = 5$ layers where every layer is a bijection using a two-layer MADE network with 50 neurons each as conditioner.

All architectures use tanh activation functions exclusively.

B.2.2 SLCP with 50 dimensions

The SLCP model with 50 dimensions uses the following generative process

$$\begin{aligned} \mathbf{y}_j \mid \boldsymbol{\theta} &\sim \mathcal{N}(\mathbf{y}_j; \mu(\boldsymbol{\theta}), \Sigma(\boldsymbol{\theta})) \text{ for } j = 1, \dots, 4 \\ \mathbf{y}_j &\sim \mathcal{N}_2(\mathbf{0}, \mathbf{I}) \quad j = 5, \dots, 25 \\ \mathbf{y} &= [\mathbf{y}_1, \dots, \mathbf{y}_{25}]^T \end{aligned} \quad (21)$$

where $\mu(\boldsymbol{\theta})$ and $\Sigma(\boldsymbol{\theta})$ are distributed as in Eqn 20.

The experimental details and the models of SNL and APT are the same as in the last paragraph.

SSNL The SSNL architecture uses a total of $K = 5$ layers. The second and forth layers are surjection layers with a reduction factor of 50%.

B.2.3 SLCP with 500 dimensions

The SLCP model with 500 dimensions uses the following generative process

$$\begin{aligned} \mathbf{y}_j \mid \boldsymbol{\theta} &\sim \mathcal{N}(\mathbf{y}_j; \mu(\boldsymbol{\theta}), \Sigma(\boldsymbol{\theta})) \text{ for } j = 1, \dots, 4 \\ \mathbf{y}_j &\sim \mathcal{N}_2(\mathbf{0}, \mathbf{I}) \quad j = 5, \dots, 25 \\ \mathbf{y} &= [\mathbf{y}_1, \dots, \mathbf{y}_{250}]^T \end{aligned} \quad (22)$$

where $\mu(\boldsymbol{\theta})$ and $\Sigma(\boldsymbol{\theta})$ are distributed as in Eqn 20.

For this model, we increased the number of MAF layers to 10 to adjust for the increased difficulty in modelling the data. Each round we simulate 10000 observations in $R = 5$ rounds.

SSNL The SSNL architecture uses a total of $K = 10$ layers. The second, forth, sixth, eighth and tenth layer are surjection layers with a reduction factor of 50%.

SNL and APT SNL/APT use a MAF with $K = 10$ layers where every layer is a bijection using a two-layer MADE network with 50 neurons each as conditioner.

B.3 Solar dynamo

The solar dynamo model uses the following generative process

$$\begin{aligned} g(y) &= \frac{1}{2}[1 + \text{erf}(\frac{y-b_1}{w_1})][1 - \text{erf}(\frac{y-b_2}{w_2})] \\ y_{i+1} &\leftarrow \alpha_i g(y_i) y_i + \epsilon_i, \quad \alpha_i \sim \text{Unif}(\alpha, \alpha + \delta), \quad \epsilon_i \sim \text{Unif}[0, \epsilon] \quad \forall i = 0, \dots, N \end{aligned}$$

For the solar dynamo model, we use MAFs consisting of 8 layers (each layer uses a MADE network with 2 hidden layers of 50 neurons each). All architectures use tanh activation functions exclusively. In each of $R = 5$ rounds we sampled $N = 1000$ observations. After having observed that SSNL already converged after 3000 data samples, we did not increase the number of rounds further.

SSNL The SSNL architecture uses a total of $K = 8$ layers. The second, forth, sixth and eighth layer are surjection layers with a reduction factor of 50%.

B.4 Additional results

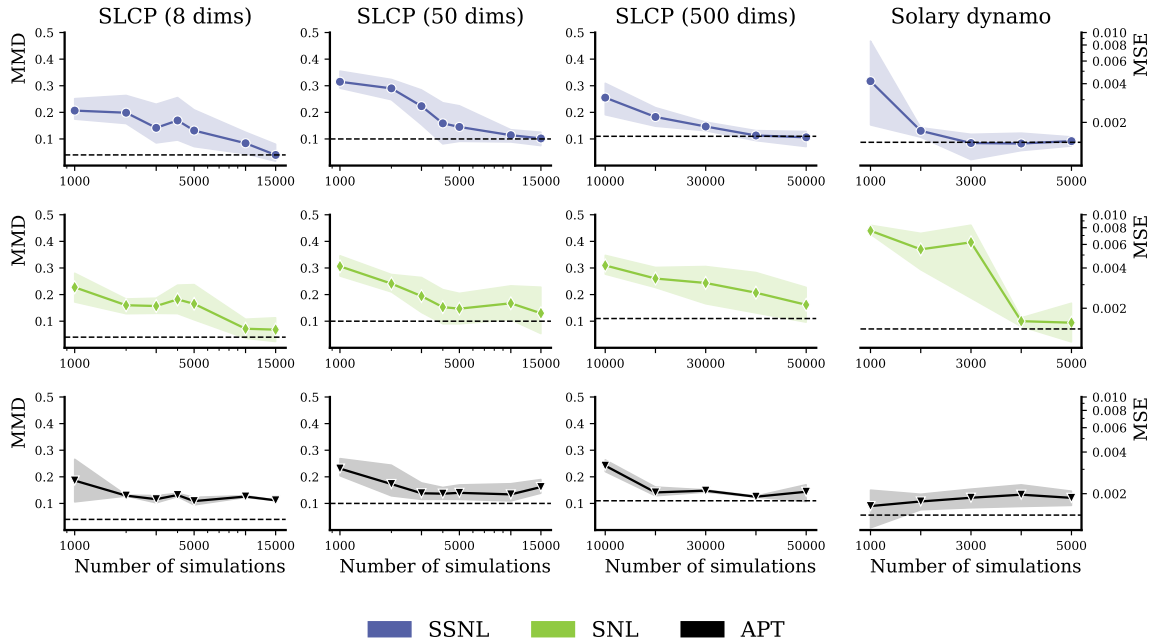


Figure 4: **Additional experimental results.** The figure uses the same experimental results as in the main paper, but has additional replicates for SNPE on the SLCP model with 50 and 500 additional dimensions.

Appendix C Source code

See the attached tar balls for source code.